Int J Earth Sci (Geol Rundsch) (2004) 93:329–340
DOI 10.1007/s00531-004-0387-6

ORIGINAL PAPER

Thuy Thi Bich Nguyen · Muharrem Satir · Wolfgang Siebel · Fukun Chen

Granitoids in the Dalat zone, southern Vietnam: age constraints on magmatism and regional geological implications

Received: 6 March 2002 / Accepted: 17 January 2004 / Published online: 6 May 2004

Abstract The Dalat zone in southern Vietnam comprises a Cretaceous Andean-type magmatic arc with voluminous granitoids and contemporary volcanic rocks. On the basis of petrographical and mineralogical studies, the granitoids were subdivided into three suites: Dinhquan, Deoca and Cana. Rocks of the Dinhquan suite are hornblende–biotite diorites, granodiorites and minor granites. The Cana suite encompasses mainly leucocratic biotite-bearing granites with scarce hornblende. The Deoca suite is made up of granodiorites, monzogranites and granites. Geochemically, the granitoids are of subalkaline affinity, belong to the high-K, calc-alkaline series, and most of them display typical features of I-type granites. This paper presents the new Rb–Sr mineral and U–Pb zircon and titanite age data for the granitoids, which establish the ages of the plutonic suites as: the Dinhquan at ~112–100 Ma, Cana at ~96–93 Ma and Deoca at ~92–88 Ma. These ages are significantly different from earlier publications, and indicate that the earliest magmatism in the Dalat zone began at ~112 Ma ago, that is ~30–50 Ma later than previously thought. Our geochronological data are also support the continuation of an Andean-type arc running from SE China via southern Vietnam to SW Borneo.

Keywords Dalat zone · Granitoids · Intrusion sequence · Rb–Sr mineral and U–Pb zircon and titanite dating · Southern Vietnam

T. T. B. Nguyen (✉) · M. Satir · W. Siebel
Institut für Geowissenschaften,
Universität Tübingen,
Wilhelmstr. 56, 72074 Tübingen, Germany
e-mail: bichthuyde@yahoo.de
Fax: +1-49-7071295713

T. T. B. Nguyen
Research Institute of Geology and Mineral Resources,
Thanh Xuan-Dong Da, Hanoi, Vietnam

F. Chen
Laboratory for Radiogenic Isotope Geochemistry,
Institute of Geology and Geophysics,
Chinese Academy of Sciences,
P.O. Box 9825, 100029 Beijing, P.R. of China

Introduction

The western Pacific region is characterised by Mesozoic and Tertiary magmatic arcs and marginal basins, such as the South China Sea (Ben-Avraham and Uyeda 1973; Taylor and Hayes 1983), Philippine Sea (Karig 1971) and Tonga-Kermadec (Karig 1970). The Dalat zone in southern Vietnam provides an example of a late Mesozoic Andean-type magmatic arc composed of voluminous granitoidic, andesitic and rhyolitic rocks. The high-K, calc-alkaline rocks in the Dalat zone are interpreted as resulting from NW-directed subduction of the western Pacific plate under the south-east Asian continental margin (Taylor and Hayes 1983). The magmatic arc associated with the Dalat zone was initially formed in south-east China in the mid Jurassic–early Cretaceous (e.g. Allen and Stephens 1971; Jahn et al. 1976, 1990), then migrated south-westward to Vietnam during the mid-Cretaceous, and continued to SW Borneo in the late Cretaceous and early Tertiary (e.g. Hamilton 1979; Fig. 1).

For more than 20 years, many Vietnamese geologists have undertaken studies on mineralogy, petrography and genesis of these granitoids (e.g. Trung and Bao 1980; Thang and Duyen 1988; Bao et al. 2000). However, most of these publications were written in Vietnamese and are largely inaccessible to the international community. Furthermore, geochemical and geochronological data for the granitoids are limited and imprecise. So far, only K–Ar and Ar–Ar mineral or whole-rock (WR) data, and a few Rb–Sr mineral ages are reported for the granitoids. These data show a large scatter in ages and discrepancies in the emplacement sequence of the granitoids in the Dalat zone.

The purpose of our study is to better constrain the emplacement ages of the granitoids and to provide a better understanding of the geological history of the Dalat zone. To achieve these aims we have performed U–Pb zircon and titanite and Rb–Sr whole-rock and mineral analyses on different rock-types of the granitoids.

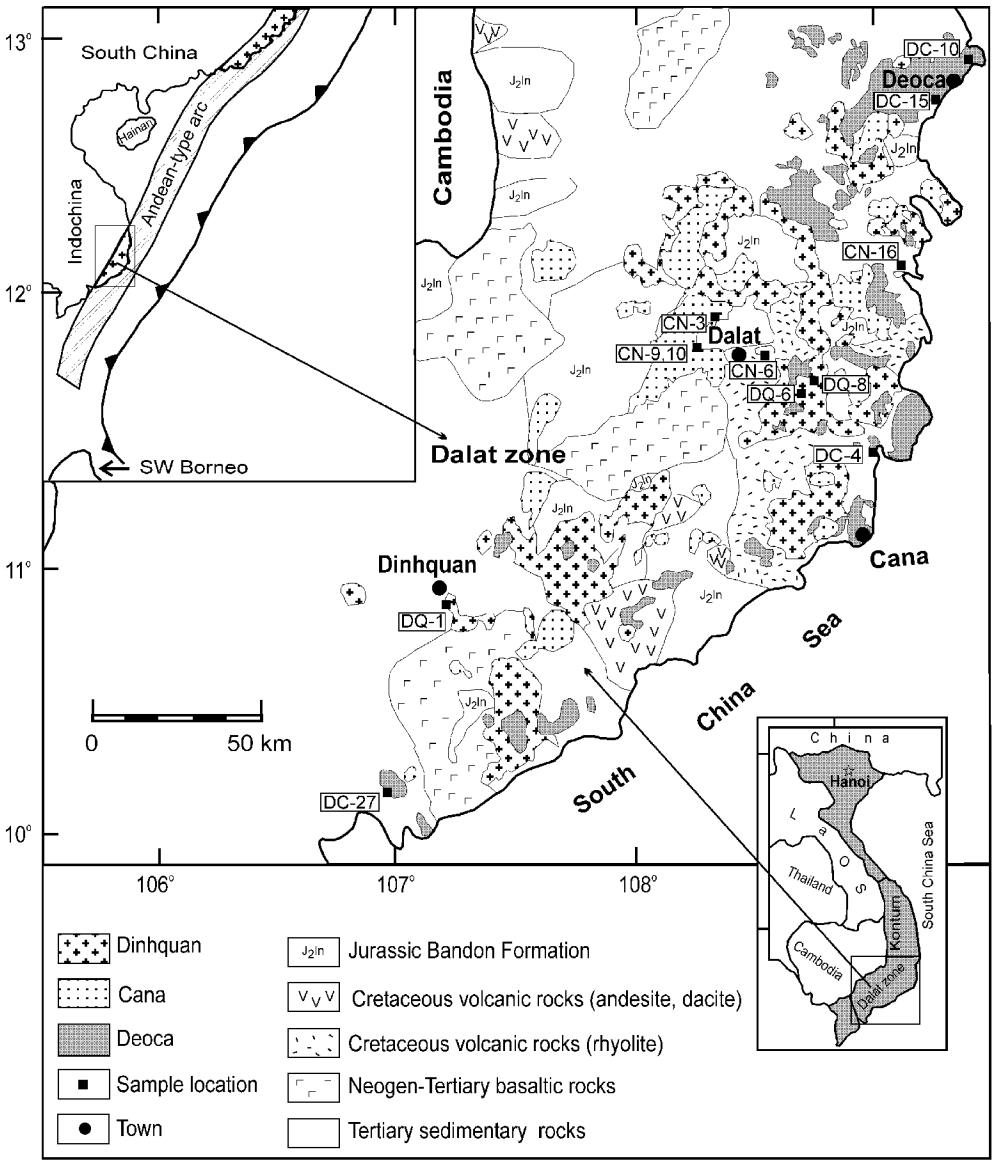

Fig. 1 Simplified geological map of the Dalat zone shows the distribution of granitoid rocks of the Dinhquan, Cana and Deoca suites (Tien et al. 1991). Letters and number beside *solid squares* denote sample numbers. The *upper inset* shows that from mid Jurassic through mid Cretaceous times the SE Asian margin was an Andean-type arc (Taylor and Hayes 1983). NW-direction subduction beneath the continent is evidenced by widespread rhyolitic volcanism and granitic intrusions along SE China (e.g. Jahn et al. 1976) and SE Vietnam. The *lower inset* shows Vietnam and location of study area

Geological setting

The Dalat zone and its extension, the Kontum massif (Fig. 1), belong to the Indochina block that consists of Gondwana-derived fragments (e.g. Metcalfe 1988, 1996; Şengör et al.1988; Hutchison 1989). The Indochina block has also been referred to as Indosinia (e.g. Helmke 1985) and Annamia (e.g. Şengör 1984). The Dalat zone is made up of Precambrian basement rocks, Jurassic sediments and late Mesozoic igneous and Cenozoic basaltic rocks (Fig. 1). The absence of Palaeozoic rocks is largely due to the Dalat zone being an emerged continent during this era (Hutchison 1989). The Kontum massif, in the north-east, and the Dalat zone are considered to have a similarly geological evolution. The basement of the Dalat zone is not exposed, but the seismic data (Khoan and Que 1984) suggest that it is composed of granulites and gneisses. K–Ar and Rb–Sr geochronological data from the granulites of the Kontum massif indicate late Paleoproterozoic (1.8–1.7 Ga; Hai 1986) and early Mesoproterozoic (1.6–1.4 Ga; Thi 1985) ages.

A thick pile of slightly folded sedimentary rocks, which are widely distributed throughout the area, overlies the basement of the Dalat zone. These rocks were formerly ascribed to the Palaeozoic Dalat series (Saurin 1935) but, in the more recent investigations, they are assigned to be the lower to middle Jurassic Bandon Formation (e.g. Luong et al. 1979). The Bandon Formation is intruded by a number of the Mesozoic granitoids. Weak contact metamorphism is commonly observed in the aureoles around the plutons, suggesting that the granitoids were emplaced at shallow depths. The uppermost part of the Dalat zone is composed of Cenozoic tholeiitic and sub-alkaline basalts that are associated with extension tectonics following the collision of the Eurasian and the Indian plate (e.g. Barr and McDonald 1981; Hoang and Flower 1998).

Table 1 Description and geochemical data of dated granitoid samples in the Dalat zone, southern Vietnam. *Bi* Biotite; *Grt* garnet; *Hbl* hornblende; *Kf* potassium feldspar; *Pl* plagioclase; *Q* quartz; *Ti* titanite; *Zir* zircon. The chemical and isotopic results are from Thuy et al (2002)

Suite	Pluton	Sample	Rock type	Texture	Mineral assemblage	(%) SiO_2	ASI	Sri	ϵ_{Nd}
Dinhquan	Dinhquan	DQ-1	Granodiorite	Medium	Q–Pl–Kf–Hbl–Bi–Zir	65.9	0.96		
	Krong	DQ-6	Granodiorite	Medium	Q–Pl–Kf–Hbl–Bi–Zir	63.8	0.92	0.07051	–1.5
	Phan	DQ-8	Granodiorite	Medium	Q–Pl–Kf–Hbl–Bi–Zir	67.3	0.96	0.7049	–0.8
Cana	Ankroet	CN-3	Granite	Medium	Q–Kf–Pl–Bi–Hbl–Zir	73.3	1.03	0.7064	–2.7
		CN-9	Granite	Medium	Q–Kf–Pl–Bi–Hbl–Zir	73.2	1.02		
		CN-10	Granite	Fine	Q–Kf–Pl–Bi–Hbl–Zir	77.8	1.05	0.7062	–2.5
	Trai Mat	CN-6	Granite	Medium	Q–Kf–Pl–Bi–Zir	77.1	1.06		
	Hon San	CN-16	Leucocratic granite	Medium	Q–Kf–Pl–Bi–Zir–Grt	76.2	1.01		
Deoca	Deoca	DC-10	Granite	Medium	Q–Kf–Pl–Bi–Zir	76.3	1.03	0.7069	–3.3
		DC-15	Granite	Medium	Q–Kf–Pl–Bi–Ti	70.7	0.97	0.7067	–2.9
	Cadu	DC-4	Granite	Coarse, Porphiric	Q–Kf–Pl–Zir	72.9	1.03		
	Nuidinh	DC-27	Granite	Coarse	Q–Kf–Pl–Bi–Zir	74.9	1.05		

On the basis of the early petrographical and mineralogical and textural studies, the granitoids have been subdivided into three plutonic suites, called the Deoca, the Dinhquan and the Cana suites (Trung and Bao 1980; Thang and Duyen 1988; Fig. 1). The granitoid rocks of all three suites mainly occur in the eastern part of the Dalat zone, parallel to the coastline to the south of the Kontum Massif. The Dinhquan suite comprises hornblende–biotite diorites, granodiorites and minor granites; the Deoca suite consists of granodiorites, monzogranites and granites; and the Cana suite is predominantly made up of biotite-bearing granites poor in hornblende. Rocks from the latter suite are characterised by small amounts of mafic minerals, in some places there are small bodies of quartz-rich granites (Hung 1999). As can be seen in the field, the Cana and Deoca granitoids clearly crosscut the Dinhquan granitoids, but contact relationships between the Cana and Deoca granitoids have not been observed. The contacts established on the Fig. 1 are speculative contacts. Some radiometric ages, obtained by the K–Ar and Ar–Ar whole-rock or mineral methods, have been reported for the three suites: ~151–118 Ma for the Dinhquan (Bao and Trung 1980), ~127–99 Ma for the Deoca (Trung and Bao1980), and ~111–78 Ma (Thang and Duyen 1988) and ~100–89 Ma (Bao et al. 2000) for the Cana suites. There are also a few Rb–Sr ages of 87–82 Ma, obtained on biotite and whole rocks, from the Deoca pluton (Lasserre et al. 1974). Almost all these ages are given without analytical procedures and supporting data tables. In some cases, whole-rock rather than mineral ages were determined.

Sample description

Representative rock types were selected from the three different plutonic suites mentioned above and their localities are shown in Fig. 1. Three Dinhquan samples DQ-1, DQ-6 and DQ-8 were collected at Dinhquan and Krong Phan plutons, respectively. Four samples of the Deoca suite were collected from three different plutonic bodies: the Deoca (DC-10 and DC-15), Cadu (DC-4) and Nuidinh (DC-27) plutons. For the Cana suite, five samples were taken. Samples CN-3, CN-9 and CN-10 were selected from the Ankroet pluton along the Tanung profile. Samples CN-6 and CN-16 are from the Traimat quarry and Honsan pluton, respectively. Rock description and geochemical data of all dating granitoid samples are given in Table 1.

Analytical techniques

Mineral separation was done following standard procedures. Rock samples of ~5–7 kg were split by employing a jaw crusher and a still roller mill. The broken material was sorted on a Wilfley table for initial density separation. Further mineral concentration was carried out with a Frantz isodynamic magnetic separator and heavy liquids (bromoform, diodomethane). Finally, zircon, titanite, biotite and K-feldspar were hand picked under a binocular microscope to avoid turbidity, inclusions and visible features that might be associated with grains affected by hydrothermal activity. Mineral purity of K-feldspar separates was checked by XRD-analyses indicating a satisfactory purification of 95–97%.

For U–Pb analysis, non-magnetic zircon fractions were selected on the basis of morphology, colour, limpidity and size. Zircon fractions were washed in hot 6 N HCl and 7 N HNO_3 for about 30 and 15 min, respectively. After spiking with a mixed ^{205}Pb-^{235}U tracer solution, zircon fractions were dissolved by 22 N HF in tiny Teflon beakers in a steel jacket digestion bomb at 200 °C for 6 days, following the vapour digestion procedure of Wendt and Todt (1991). After decomposition, HF was replaced by 6 N HCl and the bomb was heated at 180°C overnight to convert fluorite salts into more soluble chlorite salts. Separation and purification of U and Pb were performed in Teflon columns with a 40-μl bed of AG1-X8 (100–200 mesh) anion exchange resin following a similar method as described in Poller et al. (1997). Zircon standard samples (zircon 91500/Canada) were analysed during the course of this study and the results are given in Chen et al.

(2002). The same chemical procedure as used for zircon was employed for the U–Pb titanite analysis. Total procedural blanks were 10–12 pg for Pb and 1–5 pg for U. The $^{207}Pb/^{206}Pb$ zircon evaporation method was performed following the analytical technique described by Okay et al. (1996).

For investigation of internal zircon structure, representative grains were mounted in epoxy and then polished until the centre of the zircon crystal was exposed. After polishing, the mounts were coated with carbon for cathodoluminescence (CL) investigation. Polished zircon sections were analysed at the University of Tübingen by electron-microprobe using JEOL JXA-8900RL under operating conditions of 15-kV accelerating voltage, 15-nA beam current.

Rb and Sr isotopic analyses were carried out on ~50 mg of minerals (biotite, K-feldspar and plagioclase). After spiking with a mixed ^{84}Sr–^{87}Rb tracer solution, all samples were decomposed in a mixture of HF–$HClO_4$ in Teflon beakers in steel jacket bombs at 180 °C for 6 days. Rb and Sr were separated by conventional ion exchange techniques outlined in Hegner et al. (1995).

All isotopic ratios were measured in static mode on a Finnigan-MAT 262 solid-source multicollector mass spectrometer at the University of Tübingen. Pb and U samples were loaded on Re-filaments using the silica-gel technique and 1 N HNO_3, respectively. Isotopic compositions of Pb and U were measured in a single- and a double-filament configuration. Measured Pb isotopic ratios were corrected for mass discrimination of 0.10±0.03% per atomic mass unit. This value was determined by the analyses of the Pb NBS 981 standard. Sr samples were loaded on W-filaments using a Ta-HF activator and Rb samples were loaded on Re-filaments. Isotopic compositions of Sr and Rb were measured in a single- and a double-filament configuration, respectively. Measured Sr isotopic ratios were corrected for mass discrimination by normalising to a $^{86}Sr/^{88}Sr$ ratio of 0.1194. The total procedural blanks were <200 pg for Sr. During the course of this study, four analyses of NBS 987 standard gave a mean $^{87}Sr/^{86}Sr$ value of 0.710257±10 (2σ). The data were regressed using the ISOPLOT program of Ludwig (1994). All errors are quoted at the 2σ level.

Results

Zircon internal structure

The CL images of typical zircon populations from all three suites are displayed in Fig. 2. All zircon grains are euhedral and show oscillatory zoning indicating an igneous origin. Inherited zircons are not commonly observed; however, small inherited cores with brighter luminescence can be seen from zircon grains 1 and 2 of sample DQ-1. Zircons of the Dinhquan samples exhibit finely oscillatory zoning and show no or very small amounts of overgrowth. In contrast, significant overgrowths are commonly observed in zircons of the Cana rocks, particularly in sample CN-6, which contains euhedral zircons with uniform luminosity in the outer parts and brighter luminescence in the centres. Recrystallisation of the marginal portions of zircons can be inferred from the absence of zoning. Those parts are generally characterised by stronger luminescence (Pidgeon 1992), as shown in zircons from sample DC-4. CL photograph of grain 3 from sample CN-9 shows homogeneous magmatic zoning in the interior, whereas in the outer regions zoning is not observed. However, faint magmatic zoning in the outer part of this grain is revealed in backscattered electron (BSE) image (3B). The same observation is made for one grain of sample CN-10 (CL photograph 2 and BSE photograph 2B in Fig. 2).

Rb–Sr and U–Pb data

Rb–Sr analytical results are given in Table 2. Conventional U–Pb zircon and titanite data are presented in Table 3 whereas zircon evaporation $^{207}Pb/^{206}Pb$ ratios are given in Table 4. Corresponding isochron and concordia diagrams are displayed in Figs. 3a and 4 for the Dinhquan, Figs. 3b and 5 for the Cana, and Figs. 3c and 6 for the Deoca suites. Common Pb isotopic compositions of each suite were estimated from leached K-feldspar analyses (Table 5) and were used for the initial common Pb correction for all U–Pb analyses.

Table 2 Rb–Sr isotopic data for whole-rock and mineral samples of the Dalat zone granitoids. *Bi* Biotite; *Hb* hornblende; *Kf* potassium feldspar; *Pl* plagioclase; *WR* whole rock. All whole-rock data from Thuy et al. (2002). Errors of ±1% and 0.03% have been assigned to the $^{87}Rb/^{86}Sr$ and $^{87}Sr/^{86}Sr$ ratios, respectively

Sample	Rb (ppm)	Sr (ppm)	$^{87}Rb/^{86}Sr$	$^{87}Sr/^{86}Sr$
Dinhquan granodiorites				
DQ-6 (WR)	152	285	1.54	0.707490±09
DQ-6 (Bi)	685	6.5	317.51	1.196811±12
DQ-6 (Pl)	303	363	2.42	0.708746±11
DQ-8 (WR)	210	233	2.61	0.709005±10
DQ-8 (Bi)	948	2.3	1,427	2.936486±28
DQ-8 (Kf)	465	257	5.24	0.713175±12
Cana granites				
CN-3 (WR)	264	127	6.02	0.714675±10
CN-3 (Bi)	1,274	9.6	404.20	1.259758±12
CN-3 (Kf)	566	130	12.61	0.723618±01
CN-10 (WR)	351	22.1	46.44	0.770301±11
CN-10 (Bi)	1,719	12.3	427.59	1.293317±13
CN-10 (Kf)	821	28.4	84.59	0.821891±11
Deoca granites				
DC-10 (WR)	304	78.5	11.20	0.720818±10
DC-10 (Bi)	1,471	10.7	418.01	1.235257±14
DC-10 (Kf)	799	74.2	31.26	0.746238±10
DC-15 (WR)	212	302	2.02	0.709206±10
DC-15 (Bi)	1,177	11.9	296.71	1.086461±12
DC-15 (Kf)	491	287	4.95	0.712922±11

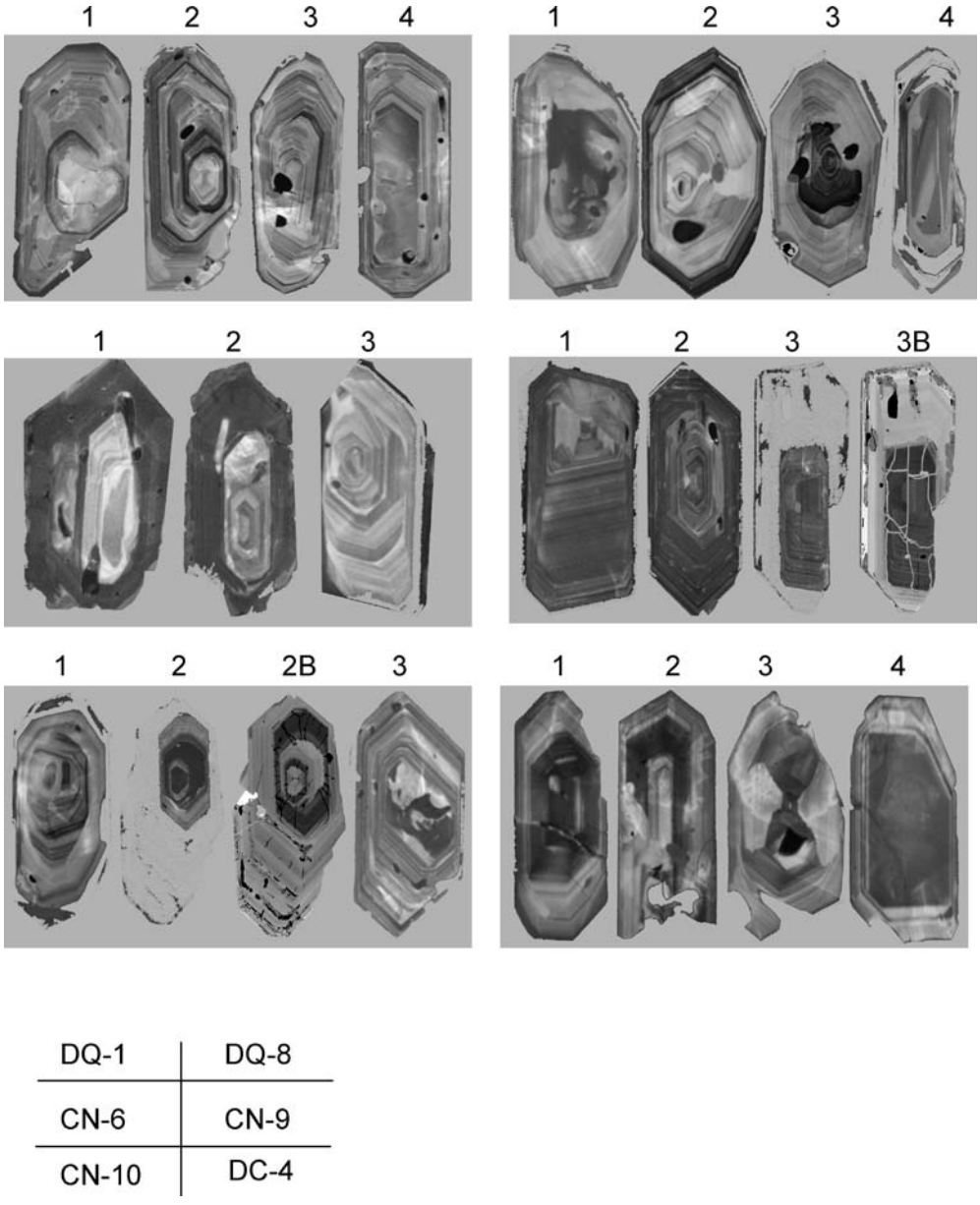

Fig. 2 Cathodoluminescence photographs of characteristic zircon populations from the Dinhquan (DQ), Cana (CN) and Deoca (DC) suites. The zircon crystals are ca. 100–150 μm long and 60–90 μm wide. Almost all zircon grains typically have prismatic morphology and oscillatory zoning indicating a magmatic origin. Magmatic zoning feature in the outer regions from the Cana samples CN-9 (grain 3) and CN-10 (grain 2) is not revealed in the CL image, but appears in the backscattered electron (BSE) images *3B* and *2B*, respectively. Note that the *dark regions* in the BSE image appear as *bright regions* in the CL image and vice versa. The photographs of grains 1 and 2 from the sample DQ-1 are typical examples for zircons containing older cores

Dinhquan plutonic suite

Granodiorite samples DQ-6 and DQ-8

All Rb–Sr WR and mineral analyses of two samples define a straight line that yields an age of ~110±1 Ma (MSWD =1.1) with an initial $^{87}Sr/^{86}Sr$ ratio of 0.70499±0.00003 (Fig. 3a). For sample DQ-8, the Pb evaporation and U–Pb conventional methods were employed. Five separately evaporated zircon grains yield a mean $^{207}Pb/^{206}Pb$ age of 109±7 Ma (Fig. 4a). To our knowledge these are the youngest rocks that have been successfully dated with this method. All of four analysed zircon fractions give concordant U–Pb ages (Fig. 4b) and define a mean $^{206}Pb/^{238}U$ age of 111.6±1.6 Ma. These ages are, within the analytical errors, identical with the Rb–Sr isochron age. The internal zircon structures as revealed by the CL images (Fig. 2) do not show relic cores. The close range of ages obtained by three different methods indicates that the rocks were emplaced at ~112 Ma.

Granodiorite sample DQ-1

Five zircon fractions were analysed from this sample (Fig. 4c). Three of them give concordant U–Pb ages of ~100 Ma. Two other fractions are discordant indicating the presence of an older Pb component, which can be observed in the CL images in the form of relic cores (Fig. 2). Regression of all five data points defines an upper intercept age of 1,834±78 Ma and a lower intercept age of 99.6±1.8 Ma. We consider the later age as the crystallisation time of this granite. The upper intercept

Table 3 Conventional U–Pb zircon and titanite analytical results of granitoids from the Dalat zone (the Dinhquan suite). All errors are two-sigma standard deviations (2σ). Common Pb isotopic compositions from K-feldspar were used for the correction of titanite and zircon analyses. The data were calculated with ISOPLOT (Ludwig 1994). *clr* Clear; *cls* colourless; *dk br* dark brown; *frg* fragments; *gr* grains; *l* long; *lt br* light brown; *md* medium; *pk* pink; *pr* prismatic; *sh* short; *sl* small; *subtr* sub-transparent; *th* thin; *thk* thick; *wh* white; *yl* yellow

Zircon description	Concentrations (ppm)				Atomic ratios			Apparent ages (Ma)		
	U	Pb_{tot}	Pb_{rad}	$\frac{^{206}PB}{^{204}PB}$	$\frac{^{206}PB^*}{^{238}U}$	$\frac{^{207}PB^*}{^{235}U}$	$\frac{^{207}PB^*}{^{206}PB}$	$\frac{^{206}PB^*}{^{238}U}$	$\frac{^{207}PB^*}{^{235}U}$	$\frac{^{207}PB^*}{^{206}PB^*}$
Sample DQ-1										
md, thk, br to cls, pr gr	690	25.4	25.1	3,118	0.03575±50	0.4246±70	0.08614±87	226.4	359.3	1341.3
l, th, tr, bl, pr, incl, gr	611	9.6	9.5	1,716	0.01543±14	0.1023±15	0.04804±58	98.8	98.9	101.2
l, th, br, subtr, pr gr	1,323	20.0	19.9	3,284	0.01558±10	0.1035±16	0.04814±49	99.8	100.0	106.2
sh, th, clr, pr gr	814	13.0	12.8	2,367	0.01563±14	0.1035±19	0.04806±77	99.9	100.0	102.2
sh, th, br, bl, tr, incl, gr	771	14.3	12.9	484	0.01690±9	0.1204±25	0.05172±99	108.0	115.5	273.1
Sample DQ-8										
l, thk, tr, pr gr	1,146	20.2	19.9	4,549	0.01730±25	0.1152±19	0.04832±53	110.6	110.8	115.0
sh, thk, br, pr subtr gr	1,689	29.2	28.9	5,576	0.01757±26	0.1178±25	0.04863±61	112.3	113.1	130.0
thk, br, frg	571	10.1	9.9	1,455	0.01742±25	0.1154±21	0.04806±331	111.3	110.9	102.2
sh, th, yl to cls, pr gr	695	12.2	12.1	1,445	0.01755±22	0.1171±21	0.04835±230	112.2	112.4	116.4
Sample CN-6										
sh, md, dk br, pr gr	4,145	58.8	57.8	1,885	0.01465±28	0.0973±22	0.04816±54	93.8	94.3	107.6
sh, th, yl, subtr gr	2,282	34.8	33.3	738	0.01489±12	0.0991±18	0.04824±78	95.3	95.9	111.1
sh, sl, cls, tr, pr gr	1,214	29.7	29.3	1,930	0.02293±12	0.1592±13	0.05037±34	146.1	150.0	212.1
sh, md, wh, tr, pr gr	1,314	27.1	26.8	2,262	0.01905±27	0.1296±24	0.04939±57	121.6	123.8	166.4
sh, md, dk br, pr gr	3,198	45.4	44.6	2,507	0.01451±10	0.0964±7	0.04814±16	92.9	93.4	106.2
Sample CN-										
sh, thk, br, pr gr	5,519	83.0	78.2	1,060	0.01495±33	0.0989±30	0.04798±222	95.7	95.8	98.3
sh, thk, br, subtr, pr gr	1,472	22.8	22.3	2,395	0.01504±22	0.1003±15	0.04841±18	96.2	97.1	119.4
sh, md, yl, pr gr	1,094	16.0	15.6	1,872	0.01464±9	0.0982±7	0.04864±21	93.7	95.1	130.5
l, md, yl to cls, pr gr	450	6.9	6.8	3,882	0.01541±6	0.1029±6	0.04843±23	98.6	99.5	120.3
l, thk, yl, subtr, pr gr	492	9.0	8.5	588	0.01692±15	0.1129±18	0.04840±67	108.1	108.6	118.9
l, thk, yl, subtr, pr gr	283	5.4	5.3	879	0.01877±15	0.1431±16	0.05529±46	119.9	135.8	424.0
sh, th, yl, subtr, pr gr	674	10.8	10.7	1,640	0.01589±14	0.1053±10	0.04808±25	101.6	101.7	103.2
Sample CN-10										
sl, lt br, tr, pr gr	5,070	81.9	72.0	484	0.01481±35	0.0988±21	0.04839±19	94.8	95.7	118.4
l, thk, br, pr gr	6,504	99.8	91.7	765	0.01475±30	0.1021±21	0.05019±67	94.4	98.7	203.8
l, th, br, subtr, pr gr	9,364	145.1	132.8	705	0.01484±30	0.0981±21	0.04799±74	94.9	95.0	98.8
sh, md, cls, clr, pr gr	8,863	134.3	121.9	674	0.01445±35	0.0961±23	0.04823±79	92.5	93.2	110.6
thk, dk br frg	8,094	127.6	113.1	532	0.01474±32	0.0979±22	0.04819±99	94.3	94.8	108.6
Sample CN-16										
l, md, wh, pr gr	14,840	213.1	200.1	1,235	0.01368±29	0.0914±19	0.04845±07	87.6	88.8	121.3
l, md, dk br, pr gr	12,380	231.2	191.0	209	0.01450±33	0.0958±21	0.04798±15	92.8	93.0	98.3
sh, thk, dk br, pr gr	7,740	139.1	111.2	273	0.01458±29	0.0964±19	0.04847±11	93.3	94.4	122.3
l, th, br yl, pr gr	14,567	223.4	207.2	845	0.01459±35	0.0960±23	0.04772±08	93.4	93.1	85.5
dr br, frg	6,601	114.9	100.1	415	0.01470±29	0.0978±19	0.04827±11	94.1	94.8	112.5
Sample DC-4										
l, thk, cls, pr gr	297	6.3	4.6	140	0.01432±17	0.0952±47	0.04823±99	91.7	92.4	110.6
l, thk, tr, cls, pr gr	106	2.6	1.6	64	0.01418±17	0.0950±45	0.04854±58	90.8	92.1	125.7
l, th, cls, tr, pr gr	187	6.5	3.0	57	0.01428±16	0.0967±45	0.04910±162	91.4	93.7	152.6
sh, th, clr, pr gr	507	8.5	7.7	225	0.01425±15	0.0948±24	0.04828±297	91.2	92.0	113.0
sh, th, pk, subtr, pr gr	584	10.5	9.4	225	0.01524±11	0.1011±32	0.04818±142	97.5	97.6	106.6
Sample DC-27										
l, thk, yl,, pr gr	548	7.7	6.2	243	0.01080±14	0.0723±15	0.04832±103	69.2	70.9	115.0
l, thk, br, subtr, pr gr	322	6.4	5.1	134	0.01447±14	0.0960±43	0.04814±240	92.6	93.1	106.2
l, thk, br, subtr gr	239	5.2	4.4	253	0.01446±16	0.0968±37	0.04857±166	92.5	93.8	127.1
sh, thk, yl to cls, pr gr	323	6.5	5.1	154	0.01434±13	0.0953±43	0.04818±381	91.8	92.4	108.1
l, thk, br, pr gr	501	8.9	8.8	270	0.01425±12	0.0939±20	0.04784± 72	91.2	91.2	91.4
Sample DC-15										
Titanite	119	4.9	3.2	77	0.01358±25	0.0893±18	0.04764±115	87.0	86.8	81.4
	110	4.6	3.0	78	0.01395±17	0.0918±16	0.04775±108	89.3	89.2	87.1
	111	4.6	3.0	78	0.01370±30	0.0900±25	0.04765±186	87.7	87.5	81.9

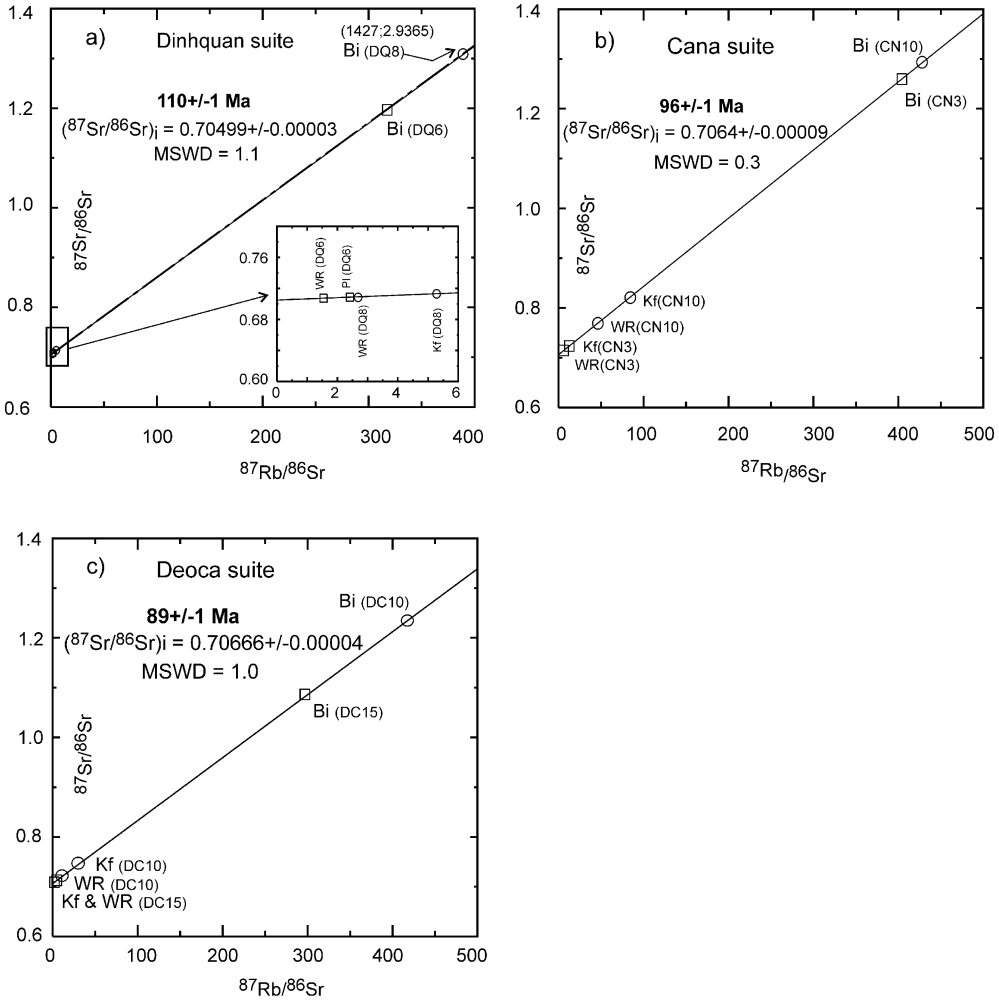

Fig. 3a–c $^{87}Sr/^{86}Sr$ vs. $^{87}Rb/^{86}Sr$ whole-rock and mineral isochron plots of data from the Dinhquan (samples DQ-6 and DQ-8), Cana (samples CN-3 and CN-10) and Deoca (samples DC-10 and DC-15) suites. *WR* Whole-rock; *Bi* biotite; *Kf* K-feldspar; *Pl* plagioclase

Table 4 Radiogenic $^{207}Pb/^{206}Pb$ ratios of evaporation single zircon grains and corresponding ages

Sample	Grain	Zircon features	Number of ratios	Mean of $^{207}Pb/^{206}Pb$ ratios	$^{207}Pb/^{206}Pb$ (Ma)
DQ-8 granodiorite	1	Thick, big	369	0.04822±18	110±9
	2	Thin, long	112	0.04822±54	110±26
	3	Thick, short	261	0.04821±17	109±9
	4	Thin, long	129	0.04817±29	107±14
	5	Thin, small	105	0.04815±22	106±11
	Mean		800	0.04820±13	109±7

Table 5 Pb isotopic compositions in K-feldspar of granitoids in the Dalat zone. Errors of the analysed ratios are <0.1%

Sample	$^{206}Pb/^{204}Pb$	$^{207}Pb/^{204}Pb$	$^{208}Pb/^{204}Pb$
DQ-8	18.449	15.536	38.310
CN-10	18.471	15.542	38.356
CN-16	18.495	15.537	38.354
DC-4	18.569	15.550	38.448
DC-27	18.487	15.532	38.343

age of ~1,834 Ma suggests the presence of an inherited Precambrian component.

Cana plutonic suite

Granite samples CN-3 and CN-10

Regression of all six data points defines a well-fitted Rb–Sr isochron that yields an age of ~96±1 Ma (MSWD =0.3) and an initial $^{87}Sr/^{86}Sr$ ratio of 0.70641±0.00009 (Fig. 3b). Four of five zircon fractions from sample CN-10 yield concordant U–Pb data with a mean $^{206}Pb/^{238}U$

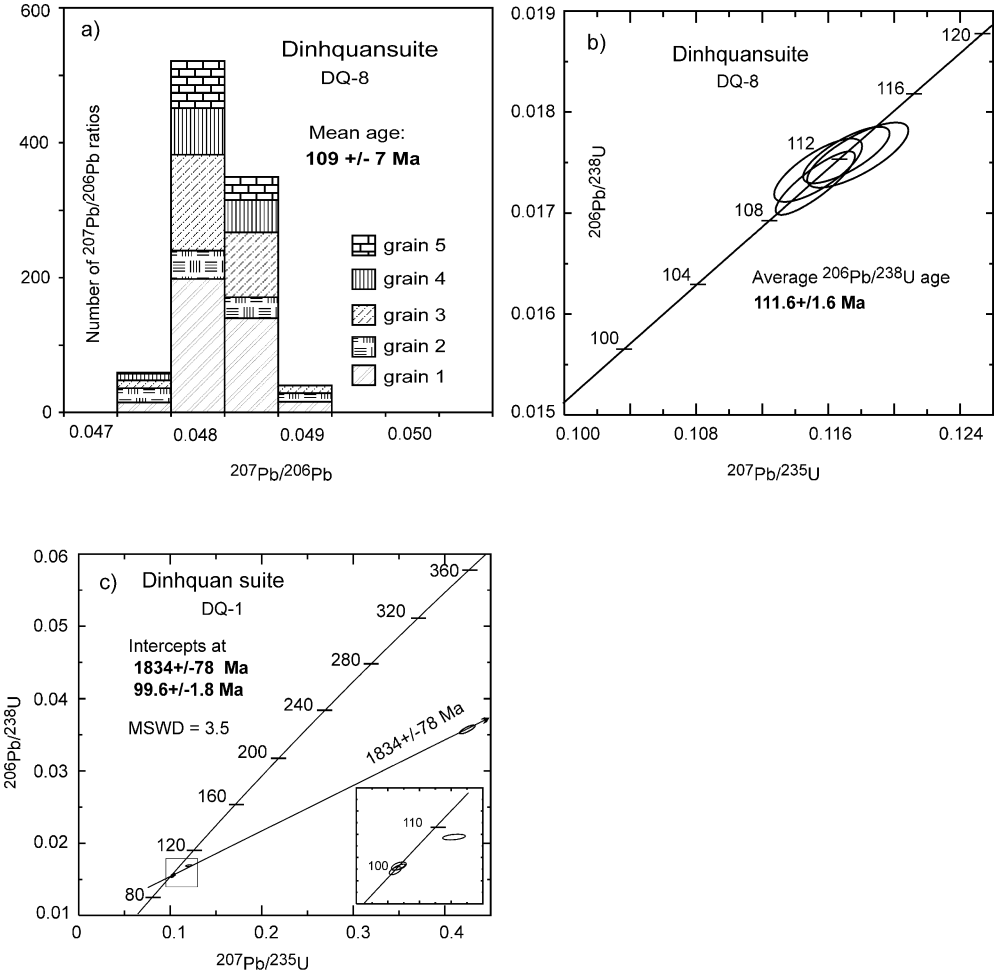

Fig. 4a–c Zircon ages for the Dinhquan granodiorite sample DQ-8 and DQ-1. **a** Histogram showing the frequency distribution of radiogenic $^{207}Pb/^{206}Pb$ ratios derived from evaporation of single zircon grains. The spectrums for five idiomorphic grains, integrated from ca. 800 ratios give an age of 109±7 Ma. **b, c** U–Pb concordia plots for zircon analyses of the Dinhquan samples DQ-8 and DQ-1, respectively. *Ellipses* indicate 2σ error

age of 94.1±2.1 Ma (Fig. 5b). The remaining fraction has an older $^{207}Pb/^{206}Pb$ age (204±31 Ma); however, it still has the same $^{206}Pb/^{238}U$ age as the other fractions.

Granite sample CN-6

This sample contains various zircon types. Most grains are broken and dark brown. Of the five fractions analysed, three are concordant and define a mean $^{206}Pb/^{238}U$ age of 94.0±1.1 Ma (Fig. 5a) that is indistinguishable from the age of sample CN-10. The two other zircon fractions, which consist of small and whitish grains, yield discordant data. Regression of these two data points forced through 94 Ma yields an upper intercept age of 317±36 Ma, which indicates the presence of an old zircon component. The concordant ages of 94 Ma are considered as emplacement age of the granite.

Granite sample CN-9

$^{206}Pb/^{238}U$ and $^{207}Pb/^{235}U$ ages of seven zircon fractions from this sample scatter between 136 and 94 Ma, but most ages cluster around 96 Ma (Fig. 5c). Four zircon fractions are concordant or nearly concordant with an average $^{206}Pb/^{238}U$ age of 96.1±1.1 Ma. Two other zircon fractions yield concordant, but older, U–Pb ages of ~108 and ~102 Ma, possibly inherited from earlier granitoids with ages similar to the Dinhquan samples DQ-8 and DQ-1, respectively. The age of ~96±1 Ma is considered to be the best estimate for the emplacement time of this granite. Another fraction is discordant and yields an upper intercept age of 1,248±66 Ma when forced through 96 Ma (discordia line; Fig. 5c).

Leucogranite sample CN-16

Five zircon fractions were analysed from this sample (Fig. 5d). Uranium concentrations are extremely high, ranging from 14,840 to 6,600 ppm. Four of five fractions analysed yield concordant U–Pb data with an average $^{206}Pb/^{238}U$ age of 93.4±2.0 Ma. Zircon grains of another fraction have the highest U-content (14,840 ppm) and yield the lowest U–Pb age of ~87 Ma. A negative correlation between the U-contents and the U–Pb zircon ages (inset in Fig. 5d) may indicate that Pb loss was probably related to U concentration. We conclude that the average

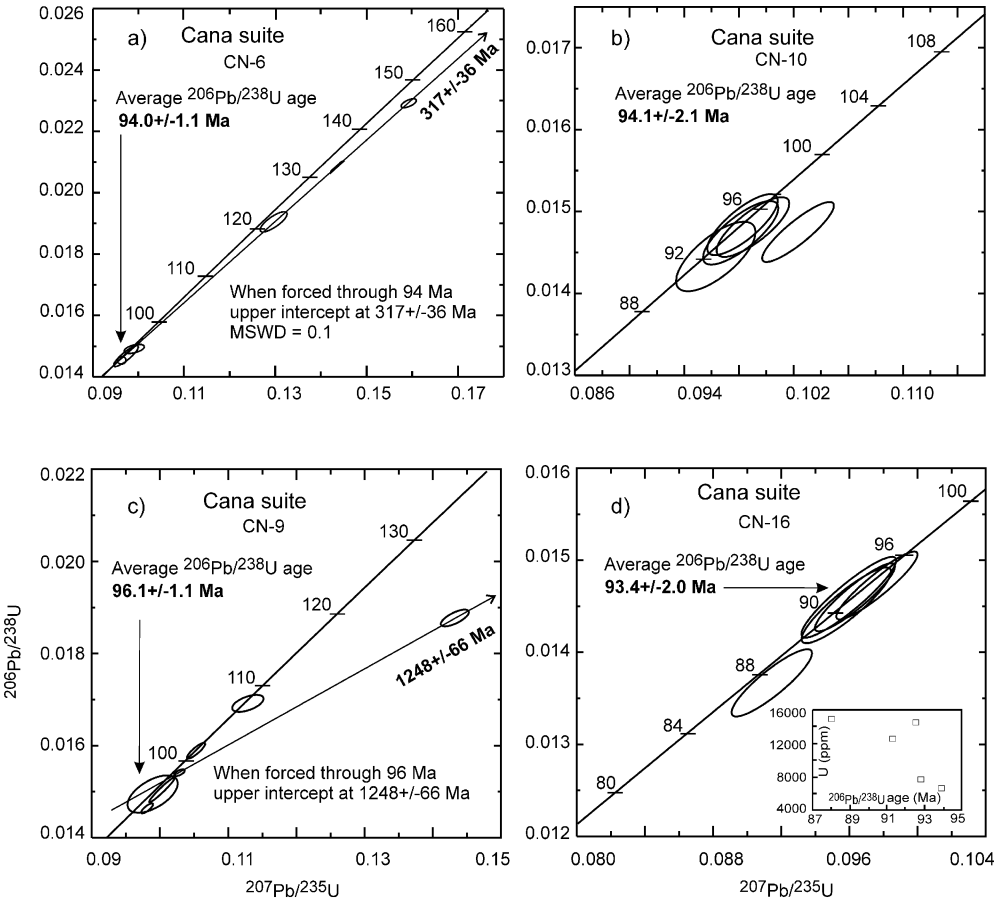

Fig. 5a–d Concordia plots showing data points of conventional U–Pb zircon analyses from the Cana granite suite. *Error ellipses* represent two-sigma errors. **a** Plot of sample CN-6, the upper intercept age of 317±36 Ma is defined by regression of two discordant data points forced through 94 Ma, which is considered as the crystallisation age of the granite. **b** Plot of sample CN-10 indicating crystallisation at 94.1±2.1 Ma. **c** Plot of sample CN-9, the upper intercept age of 1248±66 Ma is defined by regression through one discordant analysis and 96 Ma, which is considered as the crystallisation age of the granite. **d** Plot of sample CN-16 showing four concordant data points, which yield an average age of 93.4±2.0 Ma and represent the emplacement time of the granite. *Inset* shows relation between U-contents and $^{206}Pb/^{238}U$ ages. Negative correlation between these two parameters implies that Pb loss is due to high U-content of zircon

$^{206}Pb/^{238}U$ age of ~93 Ma represents the emplacement time of this granite.

Deoca plutonic suite

Granite samples DC-10 and DC-15

All six analyses of WR and minerals from the two samples define an isochron with an age of ~89±1 Ma (MSWD =1) and initial $^{87}Sr/^{86}Sr$ of 0.70664±0.00004 (Fig. 3c). Three dark-ember titanite fractions were investigated from sample DC-15 for U–Pb analysis (Fig. 6a). All data points are concordant, yielding a mean $^{206}Pb/^{238}U$ age of 88.0±1.5 Ma, which is in accord with the Rb–Sr isochron age. Note that the ages obtained for the Deoca pluton are ~40 Ma younger than those reported by Trung and Bao (1980) but are, within analytical error, in good agreement with a Rb–Sr biotite age of 87±2 Ma of Lasserre et al. (1974).

Pink granite sample DC-4

Five fractions of the best quality zircons were selected for U–Pb analysis. Compared with the Dinhquan and Cana samples, the Deoca samples contain zircons with low U and very low Pb contents (Table 3). Except for one concordant fraction with older U–Pb ages of 97 Ma, all analysed zircons yield concordant $^{206}Pb/^{238}U$ ages of ~91–92 Ma with a mean of 91.3±1.0 Ma (Fig. 6b). This age is interpreted as the emplacement age of the rock.

Pink granite sample DC-27

Zircons separated from this sample are generally brown to colourless and of poor clarity. Four of five zircon fractions are concordant and define an average $^{206}Pb/^{238}U$ age of 92.0±0.9 Ma (Fig. 6c). A further data point, which plots below the concordia curve at ~70 Ma, may indicate

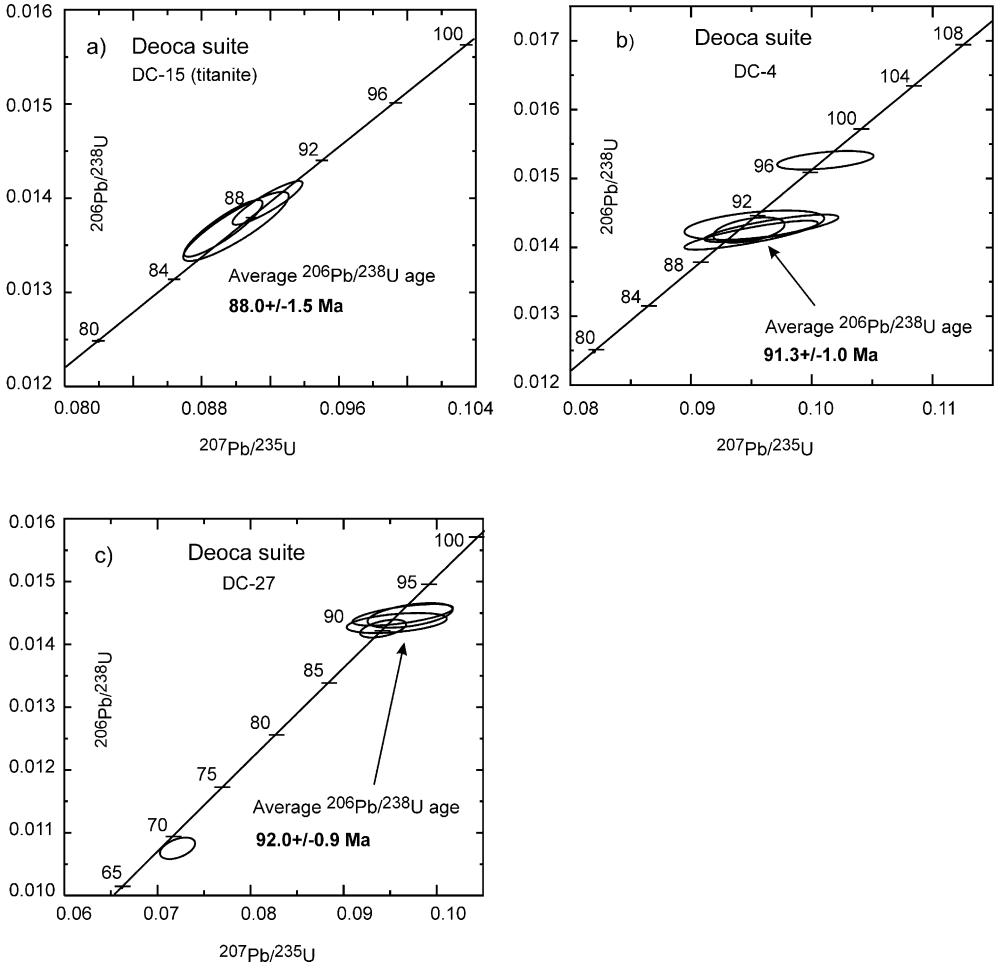

Fig. 6a–c U–Pb zircon and titanite ages for the Deoca suite. **a** U–Pb concordia diagram for titanite from the Deoca granite sample DC-15. **b** U–Pb concordia plot for zircon analyses of sample DC-4 indicating crystallisation at 91.3±1.0 Ma. **c** U–Pb concordia diagram for zircon analyses of sample DC-27. One data point plots below the concordia curve indicating Pb loss (see text for discussion)

recent Pb loss. The age of 92 Ma is considered to reflect the emplacement time of this granite.

Discussion

Constraints on the intrusion sequence

All the ages of the investigated samples recorded by different isotopic systems indicate that magmatic activity in the Dalat zone occurred during mid to late Cretaceous time. Most analysed zircon fractions plot on the concordia and yielded well-defined ages. However, some zircon fractions from the samples CN-16, and DC-27 probably suffered Pb loss and plot below the concordia curve and, hence, were excluded from mean $^{206}Pb/^{238}U$ age calculations. Negative correlation between the apparent $^{206}Pb/^{238}U$ ages and the U contents (Fig. 5d) suggest that Pb loss, at least in this sample, might have resulted from radiation damages (e.g. Davis and Krogh 2000). High U contents may facilitate a metamictisation process (e.g. Nasdala et al. 2001).

The good correspondence of the ages obtained from different radiometric methods, combined with the internal structures of zircons revealed by CL images, allows us to suggest that the emplacement time of the Dinhquan, Cana and Deoca granitoid suites were between 112 and 100 Ma, 96 and 93 Ma, and 92 and 88 Ma, respectively. These results are significantly different from previous dates. Both Rb–Sr and U–Pb ages indicate that the Dinhquan granitoids are the oldest intrusive rocks in the Dalat zone, which is consistent with observed field relationships and previous conclusions (Bao and Trung 1980). However, our data show that the rocks are ~30–50 Ma younger than the ages reported by latter authors. On the basis of few inaccurate K–Ar and Ar–Ar ages, Thang and Duyen (1988) have suggested that rocks of the Deoca suite are older than those from the Cana suite. This is, however, inconsistent with the new Rb–Sr and U–Pb ages. So far, contact relationships between the Deoca and Cana rocks have not been described. But all the dated samples from the Deoca suite gave younger ages than those from the Cana suite. The U–Pb zircon age of 93.4 Ma of sample CN-16 collected from the small, highly fractionated Honsan pluton with extremely high U-contents appears to represent a final phase in the evolution of the Cana magma, which is still somewhat older than the oldest intrusive body of the Deoca suite (Table 3). Although not all plutons from the three suites are dated, the investigated samples were chosen from different rock types, which

cover the entire compositional spectrum of the three suites, from the most primitive through to most evolved members. Therefore, we suggest that the magmatic intrusion sequence in the Dalat zone can be constrained as Dinhquan–Cana–Deoca. The shift in age from the Dinhquan suite to the others is accompanied by a change in the character of the granitoid magmatism: rocks from the Dinhquan suite are primarily I-type while most of the Cana rocks are highly fractionated I-type. Rocks of the Deoca suite exhibit a mixture of both and display porphyritic textures (e.g. Thuy et al. 2002). It is important to note that the age distribution of the granitoid intrusions in the Dalat zone are not so regular as might be expected from successive subduction in one direction of the western Pacific plate. The Deoca rocks with the youngest ages occur along the present-day coastline (Fig. 1). In other words, magmatic activity in southern Vietnam has been migrating oceanward since the early–late Mesozoic. A similar situation was reported by Jahn et al. (1976, 1990) and Guo et al. (1984) for granitoids in SE China. These authors suggested that the oceanward migration of the magmatic arc probably resulted from increase of the subduction angle. Their suggestion was supported by the angle-changing model of Zhou and Li (2000). Since the beginning of the Cretaceous, the dip of the subduction slab has increased to the normal dip resulting in decreasing width and oceanward migration of the SE China magmatic arc.

Implications for regional geology

Late-Mesozoic (112–88 Ma) magmatism in the Dalat zone produced I-type, calc-alkaline granitoid bodies. This magmatic episode is contemporary with widespread magmatic activities, for example, in eastern Asia, New Zealand, the southern Andes and western North America, which resulted from rapid sea-floor spreading in the Central and South Atlantic and throughout the Pacific (Larson and Pitman 1972). On the basis of K–Ar and Rb–Sr dates of granitoids in SE China, Jahn et al. (1976) proposed two magmatic episodes: 170–140 and 120–85 Ma. The 112–88-Ma time interval of magmatism in the Dalat zone roughly corresponds to the second thermal event of Jahn et al. (1976) or to the fourth phase of the Yenshanian orogeny (Huang 1963). This implies that the Yenshanian orogeny was not restricted to SE China, but can be extended to large areas of the eastern margin of the Asian continent, and was directly linked to rapid sea-floor spreading in the Pacific Ocean during Mesozoic time. Previous workers (e.g. Bao and Trung 1980; Tung et al. 1992) have proposed that the magmatism in the Dalat zone occurred during the early–late Jurassic. Our data suggest that the initiation of arc magmatism in the Dalat zone, and presumably the onset of subduction, started not before mid Cretaceous time. This is strong geochronological evidence for the continuation of the Andean-type arc, which was initially formed in south-eastern China during the mid Jurassic through early Cretaceous (e.g. Jahn et al. 1976, 1990; Gilder et al. 1996) extended to southern Vietnam during the mid Cretaceous and pursued to SW Borneo through the late Cretaceous and earliest Palaeocene (e.g. Gueniot et el. 1976). The question of Taylor and Hayes (1983), whether the Andean-type arc continued south of Vietnam during the Jurassic and early Cretaceous, is now clearly elucidated on the basis of our age results. The cessation of subduction in SW Borneo was associated with rifting events in south-east Asia (Taylor and Hayes 1983), induced by the collision of India with Eurasia (e.g. Tapponier et al. 1982, 1990). The onset of rifting is most likely the latest Cretaceous or early Palaeocene (65±10 Ma) (e.g. Ru and Pigott 1986; Yuan et al. 1988).

Conclusions

Rb–Sr and U–Pb ages obtained in this study provide the first reliable age constraints on the magmatic crystallisation sequence in the Dalat zone. Our data demonstrate that the arc magmatism began as early as ~112 Ma ago and lasted at least ~25 Ma. From the new data, emplacement age of three magmatic suites and the following intrusion sequence can be established as the Dinhquan at ~112–100 Ma, the Cana at ~96–93 Ma and the Deoca at ~92–88 Ma.

The Dalat granitoids are the products of multiple-pulses of magmatism that was triggered by the NW subduction of the west Pacific plate beneath the SE Asian continental margin in Cretaceous time. The geochronological results of the Dalat granitoids provide evidence for a continuation of an Andean-type arc from SE China via S Vietnam to SW Borneo.

Acknowledgements Sincere thanks are due to the Deutscher Akademischer Austauschdienst (DAAD) for the scholarship to Thuy T.B. Nguyen. We are deeply indebted to Prof. R. Altherr and an anonymous reviewer for the valuable remarks and thoughtful suggestions for improvement of the manuscript. We thank G. Bartholomä for mineral separation and E. Reitter for isotopic analyses. The help of Nguyen Thu Giao and Vu Nhu Hung for guiding Thuy T.B Nguyen in the field and for discussion is greatly acknowledged.

References

Allen PM, Stephens EA (1971) Report on geological survey of Hong Kong. Government Printer, Hong Kong

Bao NX, Trung H (1980) The distribution of intrusive magma formations, southern Vietnam (in Vietnamese). J Geol Hanoi 41:35–59

Bao NX et al. (2000) Tectonic and metallogenic map of southern Vietnam with the scale 1:1,000,000 (in Vietnamese). Department of Geology and Mineral Resources Survey, Hanoi

Barr SM, Macdonald AS (1981) Geochemistry and geochronology of late Cenozoic basalts of southeast Asia. Bull Geol Soc Am (part II) 92:1069–1142

Ben-Avraham Z, Uyeda S (1973) The evolution of the China basin and the Mesozoic paleogeography of Borneo. Earth Planet Sci Lett 18:365–376

Chen F, Siebel E, Satir M (2002) Zircon U–Pb and Pb-isotope fractionation during stepwise HF-acid leaching and geochronological implications. Chem Geol 191:155–164

Davis DW, Krogh TE (2000) Preferential dissolution of ^{234}U and radiogenic Pb from a-recoil-damaged lattice sites in zircon: implications for thermal histories and Pb isotopic fractionation in the near surface environment. Chem Geol 172:41–58

Gilder SA et al. (1996) Isotopic and paleomagnetic constraints on the Mesozoic tectonic evolution of South China. J Geophys Res 101:16137–16154

Gueniot GP, Hirlemann G, Penet B (1976) The pre-Tertiary structural evolution of Borneo. Paper presented at the 25th International geological congress. Union of Geological Science, Sydney

Guo LZ et al. (1984) Granitoids in southeastern China: their time–space distribution, tectonic framework and evolution. In: Xu KQ, Tu GZ (eds) Geology and mineralisation of granitoids. Science Technology Publishers, Yiansu, pp 38–48

Hai TQ (1986) Precambrian stratigraphy in Indochina: geology of Kampuchea, Laos and Vietnam (in Vietnamese with English abstract). Scientific Publishing House, Hanoi, pp 20–30

Hamilton WB (1979) Tectonics of Indonesian region. US Geol Surv Prof Paper 1078

Hegner E, Roddick JC, Fortier SM, Hubert L (1995) Nd, Sr, Pb, Ar and O isotopic systematics of Sturgeon lake kimberlite, Saskatchewan, Canada: constraints on emplacement age, alteration, and source composition. Contrib Mineral Petrol 120:212–222

Helmke D (1985) The Permo-Triassic paleotethys in mainland Southeast-Asia and adjacent parts of China. Int J Earth Sci 74:215–228

Hoang NT, Flower MFJ (1998) Petrogenesis of Cenozoic basalts from Vietnam: implication for origins of a diffuse igneous province. J Petrol 39:34–50

Huang CC (1963) Basic features of the tectonic structure of China (preliminary conclusion). Int Geol Rev 1:73–88

Hung VN (1999) Tin potential of high-aluminium granites (Datanky and Ankroet plutons) from the Dalat zone (in Vietnamese). MSc Thesis, National University of Ho Chi Minh

Hutchison CS (1989) Geological evolution of Southeast Asia. Clarendon, Oxford

Jahn BM, Chen PY, Yen TP (1976) Rb–Sr ages of granitic rocks in southeastern China and their tectonic significance. Bull Geol Soc Am 87:763–766

Jahn BM, Zhou XH, Li JL (1990) Formation and tectonic evolution of the SE China and Taiwan: isotopic and geological constraints. Tectonophysics 183:145–160

Karig DE (1970) Ridges and basins of the Tonga–Kermadec island arc system. J Geophys Res 75:239–254

Karig DE (1971) Origin and development of marginal basins in the western Pacific. J Geophys Res 76:2542–2561

Khoan P, Que BC (1984) Research on the deep geological structures of Kontum area (in Vietnamese). J Geol Mineral Hanoi 2:174–187

Larson L, Pitman WC (1972) Worldwide correlation of Mesozoic magnetic anomalies and its implications. Bull Geol Soc Am 88:3645–3662

Lasserre H, Fontaine H, Saurin E (1974) Geochronologie du sud Vietnam. Arche Geol Vietnam 17:1–17

Ludwig K (1994) A plotting and regression program for radiogenic-isotope data. A revision of the Open-File Report 91-445, US Geol Survey, pp 1–45

Luong TD et al. (1979) Geological map of Vietnam at 1:500,000 (in Vietnamese). J Geol Mineral Hanoi 1:5–8

Metcalfe I (1988) Origin and assembly of Southeast Asian continental terranes. In: Audley-Charles MG, Hallam A (eds) Gondwana and Tethys, vol 37. Geol Soc Spec Publ, London, pp 101–118

Metcalfe I (1996) Pre-Cretaceous evolution of SE Asian terranes. Geol Soc Spec Publ Lond 106:97–122

Nasdala L, Welzel M, Vavra G, Irmer G, Wenzel T, Kober B (2001) Metamictisation of natural zircon: accumulation versus thermal annealing of radioactivity-induced damage. Contrib Mineral Petrol 141:125–144

Okay AI, Satir M, Maluski H, Siyko M, Monie P, Metzger R, Akyüz S (1996) Paleo- and Neo-Tethyan events in northwestern Turkey: geological and geochronological constraints. In: Yin A, Harrison TM (eds) The tectonic evolution of Asia, pp 420–441

Pidgeon RT (1992) Recrystallisation of oscillatory zoned zircon: some geochronological and petrological implication. Contrib Mineral Petrol 110:463–472

Poller U, Liebetrau V, Todt W (1997) U–Pb single zircon dating under cathodoluminescence control (CLC-method): application to polymetamorphic orthogneisses. Chem Geol 139:287–297

Ru K, Pigott JD (1986) Episodic rifting and subsidence in the South China Sea. Am Assoc Pet Geol Bull 70:1136–1155

Saurin E (1935) Études géologiques sur l'Indochine du sud est (Sud Annam, Cochinchine, Cambodge-Oriental). Bull Serv Géol L'Indochine, Hanoi vol 22

Şengör AMC (1984) The Cimmeride orogenic system and the tectonics of Eurasia. Geol Soc Am Spec Paper 195

Şengör AMC, Altiuner D, Cin A, Ustaömer T, Hsü KJ (1988) Origin and assembly of the Tethyan orogenic collage at the expense of Gondwana land. In: Audley-Chalerles MG, Hallam A (eds) Gondwana and Tethys, vol 37. Spec Publ Geol Soc, London, pp 119–181

Tapponier P, Peltzer G, Le Dain AY, Armijo R (1982) Propagating extrusion tectonics in Asia: new insights from simple experiments with plasticine. Geology 10:611–616

Tapponier P et al. (1990) The Ailao Shan/Red River metamorphic belt: Tertiary left-lateral shear between Indochina and South China. Nature 343:431–437

Taylor B, Hayes DE (1983) Origin and history of the South China Sea Basin. In: Hayes DE (ed) The tectonic and geologic evolution of Southeast Asian seas and islands. Am Geophys Union Geophysics Monogr 27:23–56

Thang ND, Duyen TD (1988) Geological map of Dongnai-Benkhe region with the scale1:200,000 (in Vietnamese). Department of Geol and Mineral Resources Survey, Hanoi

Thi PT (1985) Metamorphic complexes of the Socialist Republic of Vietnam. In: Lee Sang Man (eds) Explanatory text of the metamorphic map of south and east Asia (1:1,000,000). CGMW-UNESCO, pp 90–95

Thuy TBN, Satir M, Siebel W, Vennenmann T, Long TV (2002) Geochemical and isotopic composition constraints on the petrogenesis of granitoids from the Dalat zone, southern Vietnam. J Asian Earth Sci (in press)

Tien PC, An LD, Bach LD (1991) Geology of Cambodia, Laos and Vietnam (geological map 1:1,000,000) and its explanatory note. Geol Surv Vietnam

Trung H, Bao XN (1980) The classification of intrusive magma formations, southern Vietnam (in Vietnamese). J Geol Hanoi 40:39–56

Tung NX, Tri TV, Rodnikova RD, Gatinsky YG (1992) Geodynamics of Vietnam. In: Tri TV, Tung NX (eds) Geological formations and geodynamics of Vietnam (in Vietnamese). Science and Techniques Publishing House, Hanoi, pp 203–267

Wendt JI, Todt W (1991) A vapour digestion method for dating single zircon by direct measurement of U and Pb without chemical separation. Terra Abstr 3:507–508

Yuan J, Yan KM, Chi WR, Hu CC, Chau TF (1988) Episode faulting on the Tertiary continental margin of western Taiwan. International Symposium on Geodynamic Evolution of the Eastern Eurasian Margin, Paris (abstr)

Zhou XM, Li WX (2000) Origin of Late Mesozoic igneous rocks in Southeastern China: implications for lithosphere subduction and underplating of mafic magmas. Tectonophysics 326:269–287